Iğdır Üniversitesi Fen Bilimleri Enstitüsü Dergisi, 15(4), 1329-1342, 2025
Journal of the Institute of Science and Technology, 15(4), 1329-1342, 2025

ISSN: 2146-0574, eISSN: 2536-4618

Fizik / *Physics* **DOI: 10.21597/jist.1706353**

Araştırma Makalesi / *Research Article*

Geliş tarihi / *Received*: 26.05.2025 **Kabul tarihi / *Accepted*: 30.06.2025**

Atıf İçin: Gültekin, Z. (2025). Hegzagonal Wurtzite ZnO'nun Özelliklerinin Teorik ve Deneysel Karşılaştırması. *Iğdır Üniversitesi Fen Bilimleri Enstitüsü Dergisi*, 15(4), 1329-1342.

To Cite: Gültekin, Z. (2025). Theoretical and Experimental Comparison of the Properties of Hexagonal Wurtzite ZnO. *Journal of the Institute of Science and Technology*, 15(4), 1329-1342.

Hegzagonal Wurtzite ZnO'nun Özelliklerinin Teorik ve Deneysel Karşılaştırması

Zafer GÜLTEKİN[1*]

Öne Çıkanlar:

- Deneysel veriler ve PBE tabanlı DFT analizleri, bant aralığı küçümsemesine rağmen ZnO ince filmlerdeki optik geçişlerde güçlü bir uyum göstermektedir.
- ZnO, hem teorik hem de deneysel sonuçlarda 3.2–3.4 eV aralığında belirgin UV optik aktivite ile doğrudan bant aralıklı bir davranış sergilemektedir.
- XRD ve SEM analizleri ile doğrulanan yüksek kristallilik ve homojen nanoyapı, ZnO filmlerin optoelektronik uygulamalara uygunluğunu desteklemektedir.

Anahtar Kelimeler:

- DFT
- Metal-oksit ince filmler
- Spin kaplama
- Sol-Jel

ÖZET:

Bu çalışmada, ZnO ince filmlerin optik ve elektronik özellikleri hem deneysel yöntemler hem de yoğunluk fonksiyonel teorisi (DFT) hesaplamaları kullanılarak sistematik olarak araştırılmıştır. Yapısal optimizasyonlar ve elektronik özellik analizleri, PBE değişim–korelasyon fonksiyonu kullanılarak gerçekleştirilmiştir. Sonuçlar, ZnO'nun doğrudan bant aralığına sahip bir yarıiletken olduğunu doğrulamaktadır; ancak teorik olarak hesaplanan bant aralığı değeri (0.87 eV), deneysel olarak belirlenen değerin (3.40 eV) oldukça altında kalmıştır. Bu durum, geleneksel DFT yöntemlerinin bant aralığını küçümseme eğilimine sahip olduğu yönündeki genel kabul ile uyumludur. Bu da, bant aralığının daha doğru tahmin edilebilmesi için hibrit fonksiyoneller veya GW düzeltmeleri gibi ileri düzey hesaplama yöntemlerinin gerekliliğini ortaya koymaktadır. Sayısal bant aralığı farkına rağmen, teorik ve deneysel optik parametreler arasında — soğurma katsayısı, sönümleme katsayısı, kırılma indisi ve dielektrik sabitleri dahil olmak üzere — güçlü bir spektral uyum gözlemlenmiştir. Her iki yöntem de özellikle UV bölgesinde, 3.2–3.4 eV civarında belirgin optik geçişleri göstermiştir. Ayrıca, XRD ve SEM analizleri, yüksek kristallilik ve homojen nanoyapılı bir morfolojiyi ortaya koymuştur.

Theoretical and Experimental Comparison of the Properties of Hexagonal Wurtzite ZnO

Highlights:

- Combined experimental and PBE-based DFT analysis reveals strong agreement in optical transitions of ZnO thin films, despite band gap underestimation.
- ZnO exhibits direct band gap behavior with prominent UV optical activity between 3.2–3.4 eV in both theoretical and experimental results.
- High crystallinity and uniform nanostructure of ZnO films confirmed by XRD and SEM support their suitability for optoelectronic applications.

Keywords:

- DFT
- Metal-oxide thin films
- Spin coating

Sol-Gel

ABSTRACT:

In this study, the optical and electronic properties of ZnO thin films were systematically investigated using both experimental methods and density functional theory (DFT) calculations. Structural optimizations and electrofilmnic property analyses were conducted using the PBE exchange–correlation functional. The results confirm that ZnO is a direct band gap semiconductor; however, the theoretically calculated band gap (0.87 eV) was significantly lower than the experimentally determined value (3.40 eV), consistent with the well-known underestimation problem of conventional DFT. This highlights the necessity of employing advanced computational methods such as hybrid functionals or GW corrections for precise band gap estimations. Despite the numerical discrepancy in band gap values, a strong spectral agreement was observed between the theoretical and experimental optical parameters, including the absorption coefficient, extinction coefficient, refractive index, and dielectric constants. Both methods indicated prominent optical transitions around 3.2–3.4 eV, especially in the UV region. Additionally, XRD and SEM analyses revealed high crystallinity and a homogeneous nanostructured morphology.

[1*] Zafer GÜLTEKİN (**Orcid ID:** 0000-0001-8026-0379), Bursa Uludag University, Faculty of Arts and Sciences, Department of Physics, Bursa, Türkiye

***Sorumlu Yazar/*Corresponding Author**: Zafer GÜLTEKİN, e-mail: zafergultekin@uludag.edu.tr

INTRODUCTION

Zinc oxide (ZnO), a II–VI group semiconductor, stands out in photonic, electronic, and sensor applications due to its wide band gap (~3.3 eV), high exciton binding energy (~60 meV), and chemical stability. Owing to its direct band gap structure and high transparency, ZnO finds widespread use particularly in ultraviolet (UV) photodetectors, light-emitting diodes (LEDs), transparent conductive films, and photocatalytic systems (Pearton et al., 2014; Uribe-López et al., 2021; Ilickas et al., 2023).

The fundamental electronic and optical properties of ZnO have been extensively investigated using density functional theory (DFT), which remains one of the most widely used ab initio methods in this field (Schleife et al., 2006; Janotti and Van de Walle, 2009). Although commonly used exchange-correlation functionals such as Perdew–Burke–Ernzerhof (PBE) and Local Density Approximation (LDA) often significantly underestimate the energy gap between the valence and conduction bands, they still provide qualitatively reliable results in describing properties such as band structure, optical constants, and density of states (Haffad et al., 2011; Darma et al., 2015; Mohamad et al., 2017). Therefore, to improve the accuracy of theoretical predictions for wide band gap oxides like ZnO, hybrid functionals (e.g., HSE06) or GW corrections are frequently employed (Bashyal et al., 2018; Shokri et al., 2020). In recent years, several advanced DFT studies have adopted hybrid functionals such as HSE06 and B3LYP or many-body perturbation corrections (e.g., GW) to achieve more accurate descriptions of ZnO's electronic structure, especially in doped or defect-engineered systems.

For instance, Alharshan et al. (Alharshan et al., 2023) used the HSE06 functional to study Fe-doped ZnO and reported a corrected band gap of 1.98 eV, in contrast to the severely underestimated value obtained using standard PBE. Similarly, Ouni et al. (Ouni et al., 2022) employed B3LYP to analyze sprayed ZnO thin films, obtaining theoretical band gaps (3.35 eV) that closely match experimental results (3.3 eV).

Additionally, Kholtobina et al. (Kholtobina et al., 2024) utilized DFT with hybrid functionals to investigate vanadium–phosphorus-doped ZnO films, achieving refined predictions of electronic transitions and confirming the relevance of advanced methods in tailoring ZnO band structures. These studies emphasize that hybrid and many-body methods provide not only quantitative improvements in band gap estimation but also richer insights into defect-induced states and optical properties. In addition, theoretical studies on the optical response of ZnO model the spectral distributions of parameters such as refractive index, dielectric constant, absorption, and extinction coefficients in detail, directly contributing to device design (Baizid et al., 2021; Benkrima et al., 2023).

From an experimental standpoint, ZnO is a widely studied semiconductor due to its ease of synthesis through various techniques such as sol-gel, pulsed laser deposition, RF sputtering, and chemical vapor deposition (Hasnidawani et al., 2016; Toma et al., 2025). ZnO structures fabricated in thin-film form have been extensively investigated in the literature in terms of their optical and structural properties (Muchuweni et al., 2017; Muslih et al., 2017; Krysova et al., 2024). The crystal structure, morphology, and optical responses of ZnO can vary significantly depending on several parameters such as synthesis method, processing temperature, and the use of dopants. Various studies have shown that properties such as film quality, degree of crystallinity, surface smoothness, and grain size directly affect the optoelectronic performance of ZnO (Dutta et al., 2008; Jongnavakit et al., 2012; Dubey et al., 2022). However, such experimental processes often require high-cost equipment, pure chemical precursors, and long processing times. For these reasons, theoretical calculations play a crucial role in predicting the optical and electronic properties of novel structures in advance, thereby reducing experimental burden and guiding experimental efforts. When carried out alongside experimental studies, theoretical modeling contributes to more efficient and targeted material development by saving time and resources during the production and characterization stages.

This study aims to comparatively evaluate the optical and structural properties of ZnO using both theoretical modeling and experimental characterization techniques; to examine the extent to which theoretical data correspond with experimental findings; and to assess the consistency of the employed approach on a spectral basis.

MATERIALS AND METHODS

Theoretical methodology

In this study, the electronic and optical properties of the ZnO crystal were calculated using the Quantum ESPRESSO (v7.3.1) package based on DFT. The calculations were performed using an ab initio approach based on the plane-wave basis set, and norm-conserving pseudopotentials (in UPF format) were employed to describe the interactions between atoms. The exchange-correlation interactions were treated using the PBE functional within the Generalized Gradient Approximation (GGA) framework.

During the relaxation process of the ZnO structure, the wurtzite lattice parameters were set as a = 0.3249 nm and c = 0.5206 nm. Both atomic positions and internal coordinates were optimized. The convergence threshold for atomic forces was set to 1.0×10^{-3} Ry/Bohr, and the total energy tolerance was defined as 1.0×10^{-8} Ry. The hexagonal crystal structure was specified using ibrav = 4, and the symmetry points were defined in terms of crystal coordinates.

The plane-wave cutoff energy (ecutwfc) was set to 80 Ry, while the cutoff for charge density (ecutrho) was 320 Ry. A Monkhorst-Pack scheme with an 8×8×6 k-point mesh was applied for both Self-Consistent Field (SCF) and relaxation calculations. The electronic occupations were treated as "fixed" during the electronic structure calculations, and the Methfessel-Paxton smearing method with a width of 0.01 Ry was used in the Non-Self-Consistent Field (NSCF) stage.

For band structure and density of states (DOS) calculations, 40 bands were included (nbnd = 40), and a customized set of 612 k-points along high-symmetry paths was generated for the NSCF step. The band structure was computed using the bands.x module, while the total and projected density of states were analyzed using the dos.x and projwfc.x modules, respectively. For optical properties, the epsilon.x module was used to obtain the spectral-dependent optical parameters such as absorption coefficient, extinction coefficient, refractive index, and dielectric function.

Experimental methodology

In this study, ZnO thin films were prepared using the sol-gel spin coating method. First, a ZnO precursor solution was prepared. Zinc acetate dihydrate was added to 2-methoxyethanol, used as the solvent, to achieve a 1 M molar concentration. The resulting mixture was stirred on a magnetic stirrer at 60 °C until the zinc salt was completely dissolved. To enhance the stability of the solution, monoethanolamine (MEA) was added, and the Zn:MEA molar ratio was adjusted to 1:1. Additionally, to improve the surface quality of the films, poly(vinyl pyrrolidone) (PVP) was introduced into the solution. The amount of PVP was adjusted to 0.5 wt% of the zinc content in the solution.

RESULTS AND DISCUSSION

X-ray diffraction (XRD) analysis is one of the most fundamental characterization techniques used to identify crystal structures. For metal oxides such as ZnO, it plays a crucial role in phase identification, determination of crystallinity, preferred orientation, and estimation of average crystallite size. In the XRD pattern presented in Figure 1, sharp and well-defined diffraction peaks corresponding to the typical hexagonal wurtzite structure of ZnO (space group: $P6_3mc$) are clearly observed. These peaks are in full agreement with the standard reference JCPDS card No. 36-1451, confirming that ZnO crystallized in a

pure phase with no detectable secondary phases (e.g., $Zn(OH)_2$, Zn).

The detected diffraction planes include (100), (002), (101), (102), (110), (103), (112), (200), (201), (004), and (202), corresponding to various crystallographic directions of ZnO. Among these, the (101) plane exhibits the most intense diffraction peak, indicating that the ZnO crystals show a preferential orientation along this direction. This suggests that crystal growth predominantly occurred along the (101) plane, which can significantly influence the film's morphology as well as its optical and electrical properties.

The sharpness and high intensity of the diffraction peaks indicate a high degree of crystallinity and well-oriented grains. Moreover, the narrow peak widths suggest relatively large crystallite sizes and a low level of crystal defects. The average crystallite sizes of the samples were calculated using the Debye-Scherrer formula (1) (Gültekin et al., 2023) based on the full width at half maximum (FWHM) of the peaks in the XRD patterns (Table I).

$$D = \frac{0.9\lambda}{\beta cos\theta} \quad (1)$$

where D is the crystallites size, λ is the X-ray wavelength, θ is the Bragg diffraction angle and β is the full width at half maximum.

A micro strain (ε) of films are calculated from Equation (2) (Gültekin et al., 2024).

$$\varepsilon = \frac{\beta \cos\theta}{4} \quad (2)$$

The dislocation density (δ) has been evaluated from Williamson and Smallman's formula (3) (Gültekin et al., 2024).

$$\delta = \frac{1}{D^2} \quad (3)$$

The volume of the hexagonal unit cell (V) was calculated using Equation (4) (Gültekin et al., 2024).

$$V = 0.866a^2c \quad (4)$$

Furthermore, for a given plane with Miller indices (hkl) and interplanar spacing ($d_{(hkl)}$), the lattice parameters a=b and c were calculated using Equation (5) (Gültekin et al., 2024).

$$\frac{1}{d^2{}_{hkl}} = \frac{4}{3}\left(\frac{h^2 + hk + k^2}{a^2}\right) + \frac{l^2}{c^2} \quad (5)$$

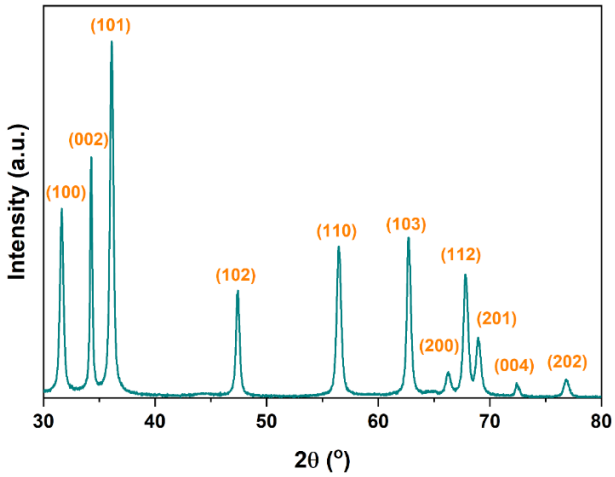

Figure 1. X-ray diffraction (XRD) pattern of ZnO

Table 1. Results calculated from XRD data

Sample	Lattice Parameters		D (nm)	D (nm)	V (pm^3)	ε (10^{-4})	δ (10^{14})
	a=b (nm)	c (nm)	XRD	SEM			(m^2)

ZnO	0.325	0.512	68	50	46.17	5.1	2.2

The scanning electron microscopy (SEM) image presented in Figure 2 was obtained to investigate the surface morphology of the ZnO thin films synthesized by the sol-gel method. Captured at approximately 30000× magnification, the micrograph reveals that the ZnO particles are homogeneously distributed across the surface, exhibit nearly spherical morphology, and contain minimal voids between the grains. This morphological structure indicates the formation of a compact film characterized by low porosity and high density.

The nearly spherical and symmetric shape of the particles suggests that the nucleation and growth processes during the sol-gel synthesis were well-controlled. Such structures promote the formation of an isotropic yet smooth surface throughout the film, effectively minimizing surface roughness. The average particle size was measured to be around 50 nm, confirming the nanostructured nature of the ZnO films (see Table 1).

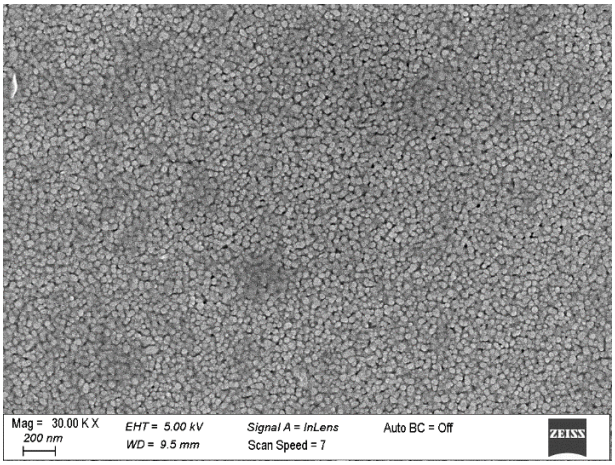

Figure 2. Scanning electron microscopy (SEM) image of the ZnO thin film

Figure 3 presents the absorption spectrum of the ZnO thin films in the energy range of 1.5–4.0 eV. The sharp rise observed around 3.2–3.3 eV corresponds to the direct band gap of ZnO, which is in good agreement with Tauc analysis and previously reported optical characterization studies in the literature (Otieno et al., 2018; Gültekin et al., 2023). This sudden increase near the absorption edge indicates the activation of direct transitions from the valence band to the conduction band. The significantly low absorbance below 3.2 eV suggests that the material exhibits high transparency in the visible region and that the photon energy is insufficient to overcome the band gap (Ayana et al., 2024).

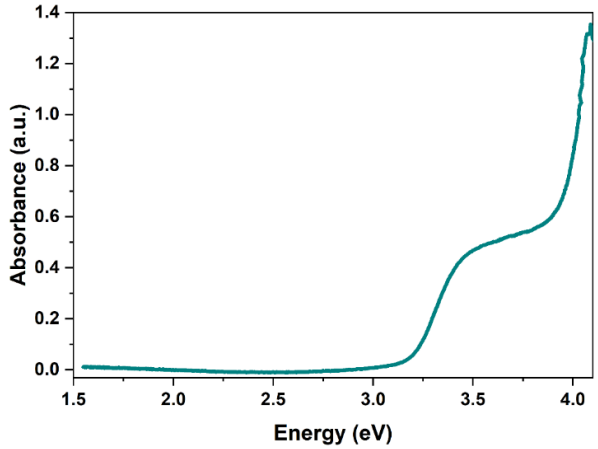

Figure 3. Absorption spectrum of the ZnO thin film

This optical behavior confirms ZnO's transparent nature and its UV-active semiconductor characteristics. The steep slope beyond 3.4 eV, particularly in the UV region, reveals that ZnO becomes

a strong absorber and exhibits high sensitivity to photon excitation. As a result, ZnO is a highly preferred material in applications such as UV photodetectors, transparent conductors, and front surface coatings for solar cells (Boruah, 2019; Wibowo et al., 2020).

Figures 4(a) and 4(b) present the experimentally measured and theoretically calculated absorption coefficients of ZnO, respectively. The absorption coefficient indicates how deeply light of a specific wavelength can penetrate into the material before being absorbed, and it is calculated using Equation (6) as provided in (Al-Ariki et al., 2021):

$$\alpha = \frac{(2.303xA)}{t} \tag{6}$$

Where t is the film thickness (The film thickness was determined to be approximately 100 nm based on the analysis of cross-sectional images obtained using a scanning electron microscope.) and A is the absorbance. In the experimental data, a sharp increase is observed around 3.2–3.3 eV, which corresponds to the direct band gap of ZnO. This value is consistent with the commonly reported band gap of approximately 3.2 eV in the literature and indicates the high crystalline quality of the material (Agarwal et al., 2019; Amakali et al., 2020).

The theoretical absorbance graph includes the variation of absorbance in the x, y, and z directions. In particular, within the energy range of approximately 1.5–4.1 eV, which corresponds to the visible region, the theoretical absorption coefficient is relatively low. This indicates that ZnO exhibits high transparency in the visible region and is a suitable candidate for UV photonic applications. Furthermore, the sharp increase beginning after 3.2 eV in the theoretical curve matches the experimental band edge, confirming the reliability of the calculations.

In the high-energy region (above 6 eV), multiple peaks observed in the theoretical spectrum correspond to electronic transitions related to Zn 3d and O 2p orbitals. Interpretations of this region are primarily intended to describe the general optical characteristics of the material for deep-UV and vacuum-UV (VUV) applications.

Figure 5(a) shows the experimental optical band gap of ZnO. The optical band gaps were determined using the Tauc equation (7) provided in (Kaushik et al., 2024):

$$\alpha h\upsilon = B(h\upsilon - E_g)^{\frac{1}{2}} \tag{7}$$

where B is a constant, hν is the photon energy, and E_g is the band gap. The band gap value obtained from the $(\alpha h\nu)^2$–energy plot was determined to be 3.40 eV. This value indicates high crystalline quality and a well-organized structure, which is largely consistent with the commonly reported range of 3.3–3.4 eV in the literature for c-axis oriented ZnO films (Safeen et al., 2023). The sharp rise in the absorbance curve confirms the presence of a direct band gap. Furthermore, this clear transition at the band edge suggests that the film contains no significant mid-gap states and exhibits a low level of structural defects.

Figure 5(b) presents the theoretical band structure of ZnO obtained using the DFT-PBE approach. According to the calculation results, the band gap was found to be approximately 0.87 eV. This value is significantly lower than the experimentally measured gap, which is a known limitation of the classical PBE functional, as it systematically underestimates the band gap. The PBE functional cannot fully correct the self-interaction error, resulting in an underestimation of the conduction band level. Therefore, rather than focusing on the absolute value of the band gap, the overall shape of the band structure, the transition type, and band dispersions are more meaningful.

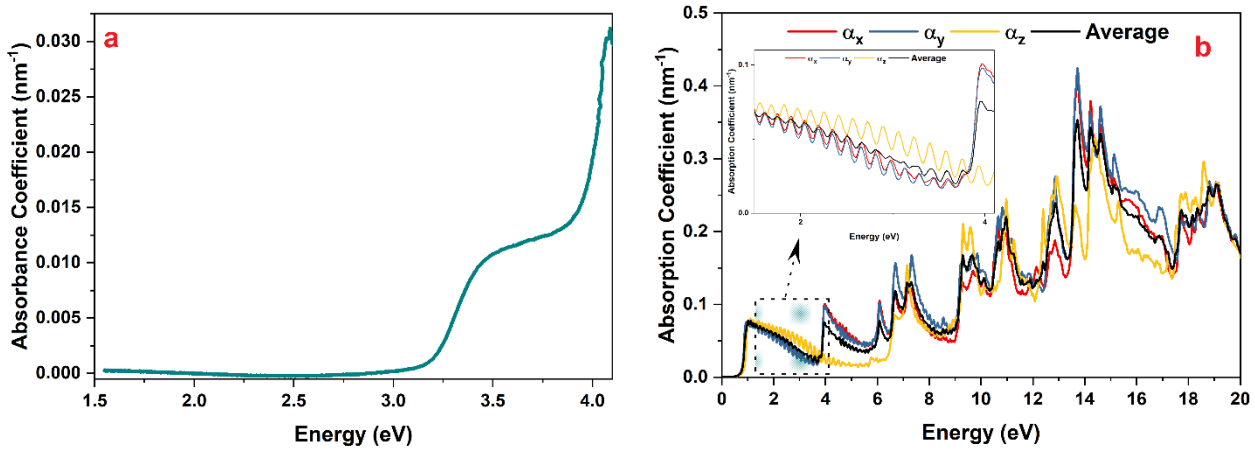

Figure 4. (a) Experimental and (b) theoretical absorption coefficients of ZnO

Upon examining the theoretical band structure, it is observed that the valence band maximum (VBM) and conduction band minimum (CBM) are located at the same k-point, confirming that ZnO is a direct band gap semiconductor. This characteristic indicates a structural agreement between the theoretical and experimental data. Additionally, the wide valence band and the parabolic nature of the conduction band suggest a favorable profile for carrier mobility. The energy bands are well-separated, especially at high symmetry points, demonstrating that the crystal symmetry is accurately reflected in the model.

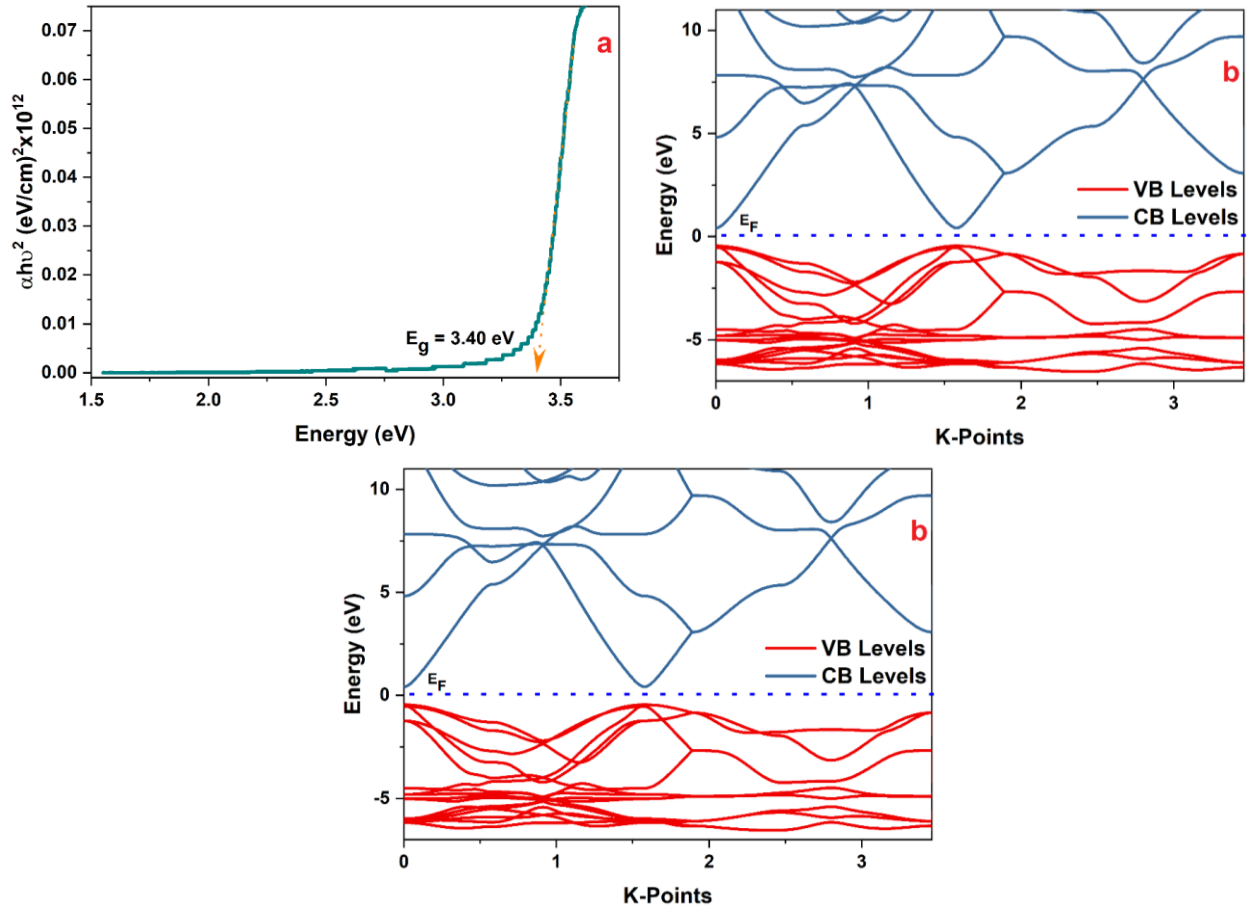

Figure 5. (a) Experimental band gap analysis of ZnO, (b) theoretical optical band structure (DFT-PBE), and (c) detailed graph of the theoretical optical band structure

Figure 5(c) shows a zoomed-in view of the band structure near the Γ point. In this region, the energy difference between the valence band maximum and conduction band minimum (0.87 eV) is more precisely visualized. The VBM is calculated to be approximately –0.45 eV, and the CBM is at +0.42 eV,

resulting in the theoretical band gap. This figure confirms that DFT calculations correctly capture the direct band gap character of ZnO, although the numerical value could be improved by employing more advanced functionals such as HSE06 or GW approaches, which are known to yield band gaps closer to experimental values.

Figure 6(a) shows the energy-dependent variation of the experimental refractive index (n) of ZnO in the photon energy range of 1.5–3.5 eV. The refractive index (n) was calculated using the formula (8) given in (Alsaad et al., 2020):

$$R = \frac{(n-1)^2 + k^2}{(n+1)^2 + k^2} \tag{8}$$

and

$$k = \frac{\alpha\lambda}{4\pi} \tag{9}$$

The extinction coefficient (k) (Hasan, 2021; Formula 9) and reflectance (R) are used to analyze the optical behavior of ZnO. At lower photon energies, the refractive index remains nearly constant, around 1.9–2.0. However, as the photon energy approaches approximately 3.2 eV, n shows a notable increase. This rise corresponds to the onset of electronic transitions near the band gap energy. These findings indicate that ZnO exhibits low optical density in the visible region, while a sharp increase is observed as the material enters the ultraviolet (UV) range. The relatively low n values in the visible spectrum confirm ZnO's high optical transparency and the minimal refraction of light within the material.

Figure 6(b) shows the theoretically calculated refractive indices of ZnO along different crystallographic directions (n_x, n_γ, n_z), along with their averaged values. The theoretical data in the 1.5–4.0 eV range show strong agreement with the experimental results. In particular, the sharp rise beginning near 3.2 eV reflects the dispersive effects caused by optical transitions around the band edge. The fact that the refractive index remains around ~1.9–2.1 in the visible region theoretically confirms ZnO's low refractive behavior in this spectral range.

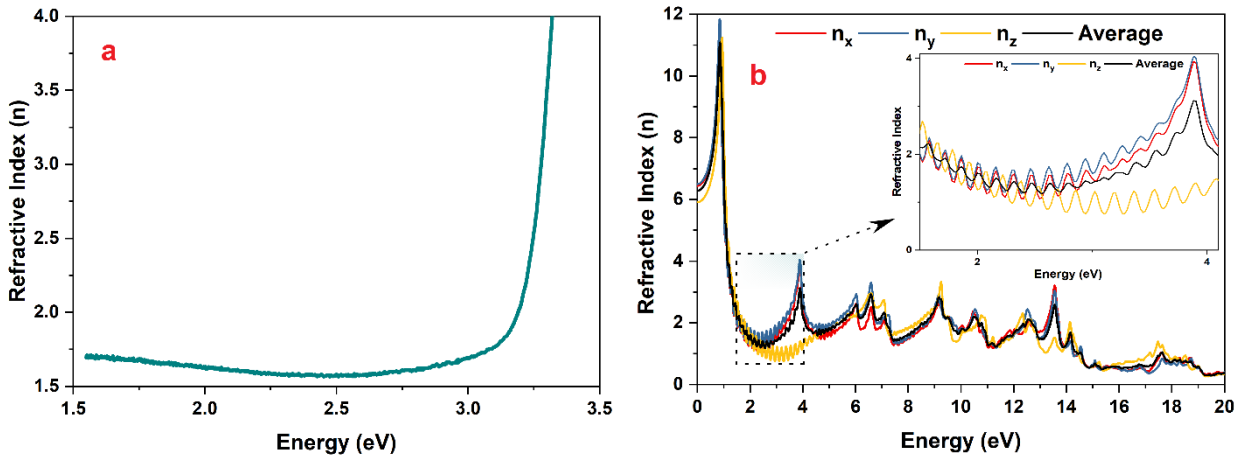

Figure 6. (a) Experimental and (b) theoretical refractive indices of ZnO

The oscillatory features observed above 6 eV in the theoretical graph are attributed to resonance effects resulting from high-energy transitions. Nevertheless, in the range of 1.5–4.0 eV, which is critical for optoelectronic applications, the refractive index remains relatively low and stable. Moreover, the consistency between theoretical and experimental curves demonstrates that ZnO is a reliable semiconductor material for optical design purposes.

Figure 7(a) shows the real part of the experimentally obtained optical dielectric constant of the ZnO thin films. The real parts of the optical dielectric constant were calculated using the formulas (10)

given in (Gültekin et al., 2023):

$$\varepsilon_r = n^2 - k^2 \quad (10)$$

Where n is the refractive index and k is the extinction coefficient. Upon examining the graph, a noticeable increase is observed around 3.4 eV. This energy threshold corresponds to the band gap of ZnO and indicates the region where the material's polarizability sharply increases upon excitation with photon energy. The relatively flat response below 3.4 eV shows that ZnO exhibits a low dielectric response in the visible region, behaving largely as a transparent material to incoming photons.

Figure 7(b) presents the theoretically calculated components of the dielectric constant of ZnO along three different crystallographic directions (ε_x, ε_γ, ε_z), as well as their averaged value. The theoretical data provide a detailed analysis of the optical response in the 0–6 eV energy range. The sharp maximum observed between 0–1 eV reflects low-energy optical transitions and atomic polarizability. This is followed by a rise around 3.3–3.5 eV, which aligns well with the experimental findings, confirming the high polarizability of ZnO near its band edge.

Across the visible region, the real part of the theoretical dielectric constant remains relatively low, indicating that ZnO tends to transmit rather than absorb light in this spectral range. Beyond 6 eV, the onset of oscillatory features reflects complex dielectric responses caused by high-energy transitions.

The transition region around 3.4 eV, clearly observed in both experimental and theoretical graphs, demonstrates a strong agreement between the two datasets. This consistency supports the reliability of both the measurement techniques and the DFT-based calculations employed in the study.

The deviations observed between the theoretical and experimental real dielectric constant (ε_r) curves in the 1.5–4.0 eV range can be attributed to the limitations of the DFT-PBE approach. Within this region, the experimental ε_r remains positive and nearly constant around ~4.5–5.0 until it sharply rises near 3.4 eV, reaching a peak of approximately 120. In contrast, the theoretical ε_r exhibits non-physical negative values, dropping to around -15 near 1.8 eV, and only begins to rise significantly after ~3.2 eV. This discrepancy stems from the PBE functional's well-known underestimation of the band gap (~0.87 eV) and its neglect of excitonic and many-body effects. Despite these differences at lower energies, both theoretical and experimental curves converge at the absorption edge (~3.4 eV), where ε_r values closely match, indicating reliable predictive performance of the model in the near-band-edge region.

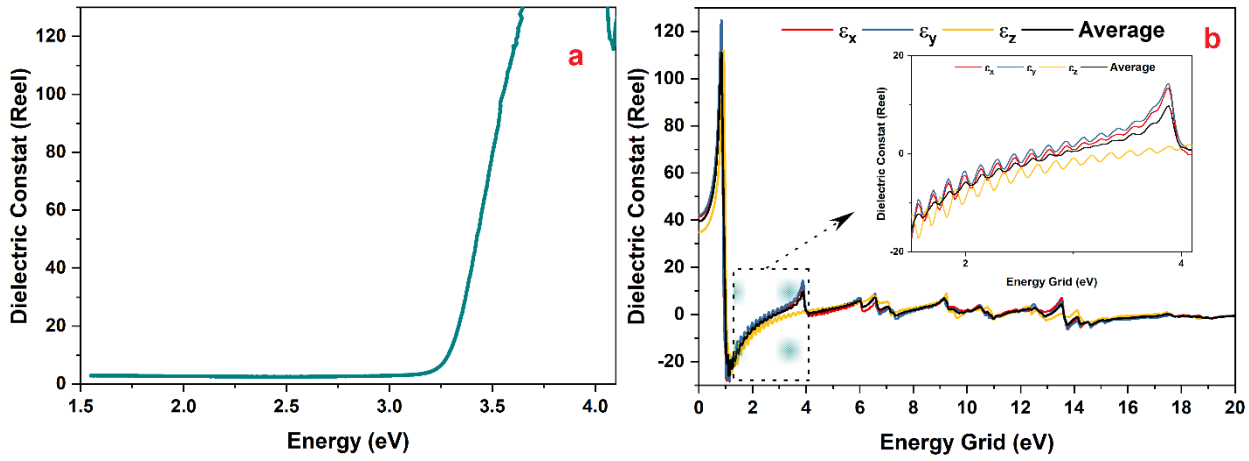

Figure 7. Experimental ε_r of ZnO, (b) theoretical ε_r of ZnO

Figure 8(a) shows the imaginary part of the measured optical dielectric constant of ZnO in the photon energy range of 1.5–4.1 eV. The imaginary parts of the optical dielectric constant were calculated using the formulas (11) given in (Gültekin et al., 2023):

$$\varepsilon_i = nk \quad (11)$$

Where n is the refractive index and k is the extinction coefficient. The pronounced increase observed around 3.4 eV corresponds to the band gap of ZnO and indicates that the photon energy has reached a level sufficient to excite electrons from the valence band to the conduction band. This sharp rise also provides optical confirmation of ZnO's direct band gap structure. Below 3.4 eV, the imaginary part of the dielectric constant remains relatively low, indicating minimal absorption in the visible region and suggesting that ZnO is highly transparent within this spectral range.

Figure 8(b) presents the theoretically calculated imaginary part of the dielectric constant of ZnO along the three crystallographic directions (ε_x, ε_γ, ε_z), along with the average value. In the energy range of 1.5–4.1 eV, covering the visible and UV regions, the rise observed particularly around 3.3–4.0 eV shows strong agreement with the experimental data. This range corresponds to the onset of photon absorption and activation of optical transitions. Although the theoretical absorption begins at slightly lower energies compared to the experimental band gap, the general transition behavior and absorption characteristics show good consistency between theoretical and experimental results.

This minor discrepancy in the 1.5–2.5 eV range can be attributed to the limitations of the DFT-PBE approach used in the calculations. For example, while the experimental imaginary dielectric constant (ε_i) remains below 1.0 throughout this range, indicating negligible absorption, the theoretical ε_i values are significantly higher—reaching ~10 at around 1.8 eV. This overestimation is mainly due to the severe underestimation of the band gap by PBE (~0.87 eV vs. experimental 3.4 eV), which causes the theoretical absorption to begin prematurely. Additionally, the lack of excitonic and many-body effects in the standard DFT framework contributes to the artificial optical transitions predicted in the sub-bandgap region. Despite this discrepancy at low energies, both experimental and theoretical curves converge around 3.4 eV, where the peak ε_i values align reasonably well, reinforcing the validity of the theoretical model near the absorption onset.

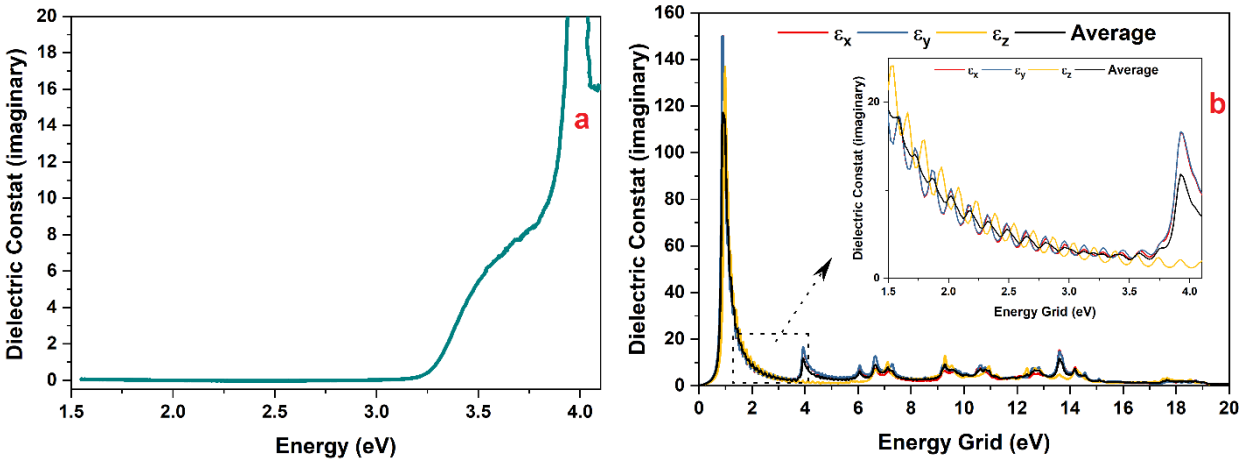

Figure 8. (a) Experimental ε_i of ZnO, (b) theoretical ε_i of ZnO

Figure 9 shows the theoretical density of states (DOS) and integrated density of states (Integrated DOS) of ZnO. In the graph, the horizontal axis represents the energy levels (eV), while the vertical axes correspond to the instantaneous density of states (green curve) and the cumulative number of electrons (red curve), respectively. The Fermi level (E_g) is set as the reference at 0 eV.

The valence band region (E < 0 eV) exhibits a dense energy distribution between –4 eV and 0 eV. The high density in this region indicates a strong contribution from O 2p orbitals, reflecting the covalent nature of ZnO and the dominant role of oxygen-derived states in the valence band. In contrast, the conduction band region (E > 0 eV) displays a more sparse and irregular energy distribution, which corresponds to the less dispersed nature of Zn 4s orbitals. The sharp peaks observed particularly between

2 and 4 eV indicate regions with a high density of available quantum states within the conduction band.

The integrated DOS curve represents the cumulative number of states as a function of energy. Its gradual increase before the Fermi level confirms the high occupancy of states in the valence band, whereas the flat behavior around the Fermi level suggests a typical "band gap closure" problem observed in conventional DFT-PBE calculations. This implies that the theoretical band gap is underestimated, and despite ZnO being a true insulator/semiconductor, it may appear metallic in such computational results.

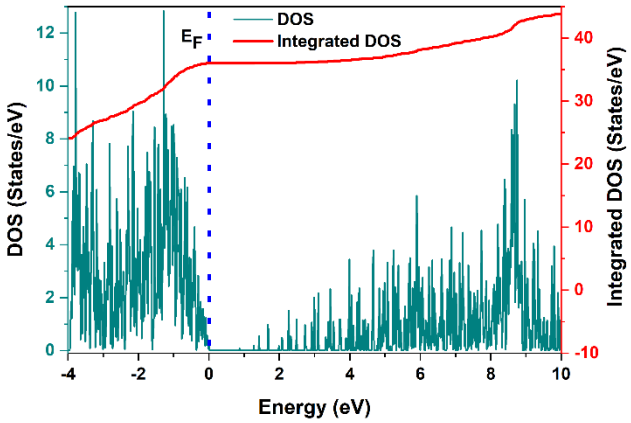

Figure 9. Theoretical density of states (DOS) of ZnO

Although this graph does not directly provide the band gap value, it is highly valuable for understanding the density distribution in the valence and conduction bands and the possible nature of electronic transitions. Particularly for ZnO's optoelectronic properties, such density analysis plays a crucial role in identifying the energy levels where optical transitions are most likely to occur.

CONCLUSION

In this study, the optical and electronic properties of ZnO thin films were comprehensively investigated through both experimental characterization and DFT-based calculations. Theoretical calculations based on the GGA-PBE approximation confirmed that ZnO is a direct band gap semiconductor; however, as widely acknowledged in the literature, PBE functionals significantly underestimate the band gap. In this study, a theoretical value of ~0.87 eV was obtained compared to the experimental value of ~3.40 eV. This underestimation is consistent with earlier reports such as Ouni et al. (2022), where standard functionals yielded smaller band gaps and hybrid functionals (e.g., B3LYP) provided results (~3.35 eV) in excellent agreement with experiment (~3.30 eV). Likewise, El Kholtobina et al. (2021) and Hallani et al. (2022) emphasize that using hybrid functionals (HSE06, B3LYP) or many-body corrections (GW) is essential to capture the accurate electronic structure of ZnO.

Despite the band gap discrepancy, a strong agreement between theoretical and experimental optical responses was observed in this study. Parameters such as the refractive index, absorption coefficient, and dielectric function all exhibited matching trends across the UV-visible spectrum, particularly near the optical absorption edge. This spectral consistency indicates that while PBE-based calculations may fall short in absolute values, they remain reliable for capturing relative optical behavior and interband transitions.

The structural and morphological characterization through XRD and SEM revealed that ZnO crystallized in the hexagonal wurtzite structure with compact nanostructured grains, in line with previous findings on sol-gel derived ZnO films. High UV transmittance and a well-defined optical band edge observed in the absorbance spectra further underscore the suitability of ZnO for optoelectronic applications. This work, therefore, supports the literature consensus that the integration of experimental

insight with improved DFT methods is crucial for understanding and tailoring ZnO's optoelectronic functionality.

Considering all results, these findings confirm that the integration of experimental techniques with DFT-based modeling—particularly when supported by advanced functionals—offers a robust framework for evaluating and engineering the optoelectronic properties of ZnO thin films.This synergistic approach is essential for guiding material development in applications such as UV photodetectors, transparent electrodes, and solar energy devices.

Conflict of Interest

The article authors declare that there is no conflict of interest between them.

REFERENCES

Agarwal, S., Jangir, L. K., Rathore, K. S., Kumar, M., & Awasthi, K. (2019). Morphology-dependent structural and optical properties of ZnO nanostructures. *Applied Physics A*, 125(8), 553.

Al-Ariki, S., Yahya, N. A., Al-A'nsi, S. A. A., Jumali, M. H., Jannah, A. N., & Abd-Shukor, R. (2021). Synthesis and comparative study on the structural and optical properties of ZnO doped with Ni and Ag nanopowders fabricated by sol gel technique. *Scientific Reports*, 11(1), 11948.

Alsaad, A. M., Al-Bataineh, Q. M., Ahmad, A. A., Albataineh, Z., & Telfah, A. (2020). Optical band gap and refractive index dispersion parameters of boron-doped ZnO thin films: A novel derived mathematical model from the experimental transmission spectra. *Optik*, 211, 164641.

Amakali, T., Daniel, L. S., Uahengo, V., Dzade, N. Y., & De Leeuw, N. H. (2020). Structural and optical properties of ZnO thin films prepared by molecular precursor and sol–gel methods. *Crystals*, 10(2), 132.

Alharshan, G. A., Aboraia, A. M., Uosif, M. A., Sharaf, I. M., Shaaban, E. R., Saad, M., ... & Elsenety, M. M. (2023). Optical band gap tuning, DFT understandings, and photocatalysis performance of ZnO nanoparticle-doped Fe compounds. *Materials*, 16(7), 2676.

Ayana, A., Gummagol, N. B., Patil, P. S., Sharma, P., & Rajendra, B. V. (2024). Nonlinear optical properties of zinc oxide thin films. *Optics & Laser Technology*, 175, 110820.

Baizid, A., Mokadem, A., Ouerdane, A., Guezzoul, M. H., Bouslama, M. H., Benchenane, H., ... & Halati, M. S. (2021). First principles calculation of structural, electronic and optical properties of K-doped ZnO. *Computational Condensed Matter*, 27, e00558.

Bashyal, K., Pyles, C. K., Afroosheh, S., Lamichhane, A., & Zayak, A. T. (2018). Empirical optimization of DFT+ U and HSE for the band structure of ZnO. *Journal of Physics: Condensed Matter*, 30(6), 065501.

Benkrima, Y., Benhamida, S., & Belfennache, D. (2023). Theoretical study of structural and optical properties of ZnO in wurtzite phase. *Digest Journal of Nanomaterials & Biostructures (DJNB)*, 18(1).

Boruah, B. D. (2019). Zinc oxide ultraviolet photodetectors: rapid progress from conventional to self-powered photodetectors. *Nanoscale Advances*, 1(6), 2059-2085.

Darma, Y., Setiawan, F. G., Majidi, M. A., & Rusydi, A. (2015). Theoretical investigation on electronic properties of ZnO crystals using DFT-based calculation method. *Advanced Materials Research*, 1112, 41-44.

Dubey, K. C., Zaidi, A., & Awasthi, R. R. (2022). Environmentally benign structural, topographic, and sensing properties of pure and Al-doped ZnO thin films. *ACS omega*, *7*(33), 28946-28954.

Dutta, M., Mridha, S., & Basak, D. (2008). Effect of sol concentration on the properties of ZnO thin films prepared by sol–gel technique. *Applied Surface Science*, *254*(9), 2743-2747.

El Hallani, G., Khuili, M., Fazouan, N., Liba, A., Abou El Makarim, H., & Atmani, E. H. (2024). Experimental and DFT investigations of Al-doped ZnO nanostructured thin films. *Chemical Physics Impact*, 8, 100648.

Gültekin, Z., Alper, M., Hacıismailoğlu, M. C., & Akay, C. (2023). Effect of Mn doping on structural, optical and magnetic properties of ZnO films fabricated by sol–gel spin coating method. *Journal of Materials Science: Materials in Electronics*, *34*(5), 438.

Gültekin, Z., Akay, C., & Altınölçek, N. (2024). Investigation of Spintronic Properties of Transition Metal Doped ZnO Thin Films Produced by Sol-Gel Spin Coating. *Sakarya University Journal of Science*, *28*(5), 1047-1058.

Haffad, S., Cicero, G., & Samah, M. (2011). Structural and electronic properties of ZnO nanowires: a theoretical study. *Energy Procedia*, *10*, 128-137.

Hasan, B. A. (2021, March). Investigating the Effect of ZnO on the Structural and Optical Properties of $(MgO)_{1-x}$ $(ZnO)_x$ via Pulsed Laser Deposition. In *Journal of Physics: Conference Series* (Vol. 1829, No. 1, p. 012032). IOP Publishing.

Hasnidawani, J. N., Azlina, H. N., Norita, H., Bonnia, N. N., Ratim, S., & Ali, E. S. (2016). Synthesis of ZnO nanostructures using sol-gel method. *Procedia chemistry*, *19*, 211-216.

Ilickas, M., Marčinskas, M., Peckus, D., Mardosaitė, R., Abakevičienė, B., Tamulevičius, T., & Račkauskas, S. (2023). ZnO UV sensor photoresponse enhancement by coating method optimization. *Journal of Photochemistry and Photobiology*, *14*, 100171.

Janotti, A., & Van de Walle, C. G. (2009). Fundamentals of zinc oxide as a semiconductor. *Reports on progress in physics*, 72(12), 126501.

Jongnavakit, P., Amornpitoksuk, P., Suwanboon, S., & Ratana, T. (2012). Surface and photocatalytic properties of ZnO thin film prepared by sol–gel method. *Thin Solid Films*, *520*(17), 5561-5567.

Kaushik, V., Bhardwaj, K., Kumar, D., Kumar, M., & Sharma, S. K. (2024). Effect of various processing parameters on the properties of ZnO thin films. *Hybrid Advances*, *7*, 100295.

Kholtobina, A. S., Kovaleva, E. A., Melchakova, J., Ovchinnikov, S. G., & Kuzubov, A. A. (2021). Theoretical investigation of the prospect to tailor ZnO electronic properties with VP thin films. *Nanomaterials*, 11(6), 1412.

Krysova, H., Mansfeldova, V., Tarabkova, H., Pisarikova, A., Hubicka, Z., & Kavan, L. (2024). High-quality dense ZnO thin films: work function and photo/electrochemical properties. *Journal of Solid State Electrochemistry*, *28*(8), 2531-2546.

Mohamad, A. A., Hassan, M. S., Yaakob, M. K., Taib, M. F. M., Badrudin, F. W., Hassan, O. H., & Yahya, M. Z. A. (2017). First-principles calculation on electronic properties of zinc oxide by zinc–air system. *Journal of King Saud University-Engineering Sciences*, *29*(3), 278-283.

Muchuweni, E., Sathiaraj, T. S., & Nyakotyo, H. (2017). Synthesis and characterization of zinc oxide thin films for optoelectronic applications. *Heliyon*, *3*(4).

Muslih, E. Y., & Kim, K. H. (2017, July). Preparation of zinc oxide (ZnO) thin film as transparent conductive oxide (TCO) from zinc complex compound on thin film solar cells: A study of O2 effect on annealing process. In *IOP Conference Series: Materials Science and Engineering* (Vol. 214, No. 1, p. 012001). IOP Publishing.

Ouni, B., Larbi, T., & Amlouk, M. (2022). Vibrational, Electronic and Structural Study of Sprayed ZnO Thin Film Based on the IR-Raman Spectra and DFT Calculations. *Crystal Structure Theory and Applications*, 11(2), 23-38.

Otieno, F., Airo, M., Erasmus, R. M., Billing, D. G., Quandt, A., & Wamwangi, D. (2018). Effect of thermal treatment on ZnO:Tb^{3+} nano-crystalline thin films and application for spectral conversion in inverted organic solar cells. *RSC advances*, *8*(51), 29274-29282.

Pearton, S. J., & Ren, F. (2014). Advances in ZnO-based materials for light emitting diodes. *Current Opinion in Chemical Engineering*, *3*, 51-55.

Safeen, K., Safeen, A., Arif, D., Shah, W. H., Ali, A., Ali, G., & Ahmad, K. S. (2023). Tuning the optical properties of ZnO by Co and Gd doping for water pollutant elimination. *Water*, *15*(8), 1470.

Schleife, A., Fuchs, F., Furthmüller, J., & Bechstedt, F. (2006). First-principles study of ground-and excited-state properties of MgO, ZnO, and CdO polymorphs. *Physical Review B-Condensed Matter and Materials Physics*, 73(24), 245212.

Shokri, A., Yazdani, A., & Rahimi, K. (2020). Possible bandgap values of graphene-like ZnO in density functional theory corrected by the Hubbard U term and HSE hybrid functional. *Materials Today Communications*, *22*, 100756.

Toma, F. T. Z., Rahman, M. S., & Maria, K. H. (2025). A review of recent advances in ZnO nanostructured thin films by various deposition techniques. *Discover Materials*, *5*(1), 60.

Uribe-López, M. C., Hidalgo-López, M. C., López-González, R., Frías-Márquez, D. M., Núñez-Nogueira, G., Hernández-Castillo, D., & Alvarez-Lemus, M. A. (2021). Photocatalytic activity of ZnO nanoparticles and the role of the synthesis method on their physical and chemical properties. *Journal of Photochemistry and photobiology A: Chemistry*, *404*, 112866.

Wibowo, A., Marsudi, M. A., Amal, M. I., Ananda, M. B., Stephanie, R., Ardy, H., & Diguna, L. J. (2020). ZnO nanostructured materials for emerging solar cell applications. *RSC advances*, *10*(70), 42838-42859.